

Ten Port and Fourteen Port MIMO Arrays for 5G Smart Phone Applications in a Sub 6 GHz band

Tamer Gaber Abouelnaga

Microstrip Circuits Department, Electronics
Research Institute (ERI), Giza, Egypt
tamer@eri.sci.eg

Ibrahim Zewail

Higher Institute of Engineering and
Technology, Kafrelsheikh, Egypt
ibrahimzewail@kfs-hiet.edu.eg

Mona Shokair

Faculty of Electronic Engineering,
Menoufia, Egypt
mona.sabry@el-eng.menoufia.edu.eg

Abstract— In this paper, two designs of ten port and fourteen port Massive Multiple-Input–Multiple-Output (MIMO) arrays are proposed for the Fifth Generation (5G) cellphone applications. A dual-band ring loop antenna is proposed to cover the LTE band 42 (3.4 – 3.6 GHz), LTE band 43 (3.6 – 3.8 GHz), and LTE band 46 (5.15 – 5.925 GHz). The proposed arrays are designed with changing the battery position and exploiting the space to add more antennas. Also, better isolation may be achieved concerning the use of spatial diversity methods on the antenna components. To achieve higher isolation, the substrate is formed as the loop antenna elements are printed on a separated dodecagon FR4 substrate with different orientation angles. The proposed designs achieve isolation better than -26 dB. Envelope Correlation Coefficient (ECC) based on S-parameters is found to be better than 0.005 in LTE band 42/43 and 0.006 in LTE band 46. Also, the ECC is calculated based on far-field radiation patterns and is found to be less than 0.2 in LTE band 42/43 and less than 0.12 in LTE band 46. The channel capacities are attained, the 10×10 MIMO achieve 57.6 bps/Hz, and the 14×14 MIMO achieve 72 bps/Hz. Additionally, The Specific Absorption Rate (SAR), Diversity Gain (DG), and the effect of frame insertion on the proposed array are also discussed.

Keywords—5G, Ergodic Capacity, MIMO, SAR, Smartphones.

I. INTRODUCTION

Nowadays, the next generation of 5G communication networks has a new vision of offering exceptionally high data rates in the GHz range, better capacity, lower latency, 100 percent coverage, and a sufficient rise in user Quality of Service (QoS).[1], [2]. Furthermore, today's smartphones provide a wide range of applications. As a result, smartphones should be able to increase signal transmission performance and operate in many bands. Furthermore, large MIMO approaches can substantially enhance channel capacity and spectrum efficiency [3].

Some MIMO antenna designs for 5G cell phones have recently been presented. Massive MIMO arrays, among the several methods that can be used, can increase channel capacity and spectrum efficiency. In reality, the MIMO approach, which incorporates a high number of antenna elements into the smartphone device and the base station, is the crucial technology for future 5G networks. Cramming as many antennas into a small space will reduce efficiency and reduce isolation. The traditional 2×2 MIMO arrays were utilized in 4G Long Term Evolution (LTE) networks. It, on the other hand, cannot afford large data rates. As a result, arrays of 6×6 MIMO, 8×8 MIMO, 10×10 MIMO, or 12×12 MIMO are now required [4]. LTE 42 (3.4–3.6 GHz), LTE 43 (3.6–3.8 GHz), and LTE 46 (5.15–5.925 GHz) are

the three most often used bands in 5G. LTE 42 is a potential spectrum band for 5G Massive MIMO, and it has been employed in a variety of MIMO antenna array designs [3].

The LTE band 46 has been chosen as a potential band for 5G MIMO architecture. Some MIMO antenna array designs for 5G cell phones have recently been presented. The researchers offered several numbers of antenna elements to cover one 5G band [4] - [5], two 5G bands [3], or three 5G bands [6]-[7]. In reference [3], eight ports array design for a 5G smartphone was proposed. The antenna element is a dual-band antenna composed of a monopole antenna (U-shaped) with an open slot antenna (L-shaped). The design covered both LTE band 42 and LTE band 46. It obtained total efficiency of more than 50%, isolations >12 dB, ECC coefficients < 0.1, and channel capacity equal to 39.7 bps/Hz. But more antenna elements can be added in the same size. Another design was proposed in [5], where four compact self-decoupled antennas were used in 150×73 mm² ground size, covering only the LTE band 42. The antenna pair were self-decoupled with isolation of 17 dB, and ECC < 0.1. But that design used a small number of antennas, and the LTE band 46 is not covered.

In reference [6], a design of a MIMO array with 12 antenna elements was used in 150×80 mm² ground size. It used three types of antennas: an inverted π -shaped antenna and two open slot antennas that are longer and shorter inverted L-shaped. The design achieved an isolation -12 dB, and total efficiency > 40%, ECC < 0.15, and ergodic capacity about 34 bps/Hz. But not the twelve antennas were used to cover both LTE bands 42/43 and 46. In Ref. [7], a design of an 8-antenna array for 5G applications. The design covers the entire 5G NR Band (n77/n78/n79) and LTE Band 46. It demonstrated an ECC of < 0.1, an efficiency of more than 41%, and a peak channel capacity of 39 bps/Hz. Another design was proposed in [8], which used 8 antennas to cover only LTE band 42, achieving isolation equal to 20 dB and ECC < 0.0125. But, the high band LTE 46 is not covered and more antennas can be added. In Ref. [9], and eight ports array in a metal frame design was proposed to cover LTE bands 41/42/43. It achieved isolation about 11 dB, ECC values < 0.2. But, the high band LTE 46 is not covered. In Ref. [10], A MIMO antenna array for metal-frame smartphone applications using 5G New Radio (5G NR) is suggested. The MIMO array is created by inserting eight identical antennas (Ant1~ Ant8) into the smartphone's metal frame. Each antenna element is a slot antenna, consisting of an L-shaped open slot and a 50 microstrip feed line, with an antenna efficiency of 50–82 percent and an ECC of 0.11.

Ref. [11], demonstrated an ultra-wideband MIMO system with high isolation for use in 5G metal frame smartphones. On the metal, there are C-shaped and T-shaped slots. To increase the isolation of the MIMO antenna system there is a modified H-shaped slot between each antenna element. The MIMO array has a 58 % bandwidth extending from 3.3 to 6 GHz, with isolation exceeding 18 dB and the ECC is below 0.05.

Ref. [12], proposes a massive MIMO-enabled antenna terminal for future 5G communications. It houses ten identical antennas, where each antenna is a slot on the ground plane fed with an inverted-F stub (IFS) feed on the top plane. This structure produces a wide impedance bandwidth (IBW) by combining different resonant modes to cover all the proposed bands in the range of 3.2–6.1 GHz for 5G mobile communications. Ref. [13], presents a 4×4 MIMO antenna array with wideband performance. It is composed of two PIFA-pairs: a planar inverted-F antenna (PIFA) with an inverted-T-shaped open slot. The proposed PIFA covers the 5G NR frequency bands: n77/n78/n79 and LTE band 46. Additionally, the isolation between two PIFA-elements in a PIFA-pair is higher than 10 dB across the broadband.

A self-isolated 10-element antenna array is proposed in [14], to cover the LTE band 42 for 5G massive MIMO smartphone applications. The antenna structure is a shorted loop antenna resonating at half-wavelength mode. It is a printed, shorted, and compact loop antenna with a total footprint area of $6 \times 6.5 \text{ mm}^2$ (14.3×13.2). A small capacitive coupling flag-shaped strip is used to excite the antenna. The design shows isolation better than -10 dB, and total efficiency $> 65\%$ ECC below 0.055. Ref. [15], presents a six-port MIMO array for hybridization of 5G and LTE-A 4G smartphone applications. Each antenna element consists

of a step-shaped feed line and an annular ring shape. The design covers LTE bands 40/41, 5G New Radio sub 6 GHz n77/n78/n79, and WLAN frequency bands. It achieved isolation of -20dB, gain $> 3\text{dBi}$, efficiency $> 70\%$, ECC < 0.01 and, channel capacity equal 32 bps/Hz.

In Ref.[16], an inverted L-shaped monopole eight elements MIMO system is presented. The design consists of eight inverted L-shaped elements and parasitic L-shaped strips extending from the ground plane. The system is designed to cover the band 3.3 – 3.7 GHz. The design achieved isolation greater than 15 dB, a gain of 4 dBi, ECC < 0.1 , and a channel capacity of 38.1bps/Hz. Table 1 shows a comparison between different MIMO antenna arrays for 5G smartphone applications.

In this paper, 10 port and 14 port multi-band MIMO antenna arrays are proposed for 5G smartphones to cover both the LTE bands 42/43 and LTE 46. Firstly, ten ring loop antenna elements are integrated into the PCB and the cell phone battery is designed to be in the corner of the handset. The proposed 10×10 MIMO array is simulated and then fabricated. Secondly, we modified the 10 port MIMO array to be 14 port array by removing the phone battery from the corner and adding four antenna elements. The CST Microwave Studio is used to obtain the simulated results. The S-parameters are calculated and compared with the measured counterpart. The proposed designs achieve vital results in terms of good isolation below -26 dB, lower ECC value, and high ergodic channel capacities across the operating bands. Additionally, SAR, DG values, and the effect of frame insertion on the proposed array are also discussed.

TABLE 1 A comparison between different MIMO antennas for 5G MIMO smartphone applications

Reference	No. of Elements	Antenna Type	Element Size (mm)	Element separation	Bandwidth (GHz)	Isolation (dB)	Element Efficiency	ECC at resonance	Ground Size (mm^2)	Method Of ECC Calculation
[6]	12	Inverted π -shaped antenna,	14×13	10	3.4–3.8 (-6 dB)	12 dB	82 %	< 0.15 (LB)	150×80	Measured Complex Electric Field
		Longer inverted L-shaped open slot antenna	15.5×10.5		5.15–5.925 (-6 dB)		75 %	< 0.1 (HB)		
		Shorter inverted L-shaped open slot antenna.	15.5×7.2							
[3]	8	L-shaped open slot antenna and a U-shaped monopole antenna.	L-shaped (10.2×4) U-shaped (14.9×4.6)	21.7	3.4- 3.6 (-10 dB)	12 dB	68%	< 0.1 (LB)	150×75	Three-Dimensional (3D) Electric Field Patterns
					5.15- 5.925 (-6 dB)		72%	< 0.04 (HB)		
					LTE band 46		82 %			
[9]	8	Monopole antenna	22×17	8.5	41/42(2.496-2.69)	10 dB	66 %	< 0.2 (LB)	150×76.6	Measured 3D Complex Electric Field Patterns
					43(3.4- 3.8)		59 %	< 0.05 (HB)		
					LTE 46 (-6 dB)		75 %			
[8]	8	T-shaped feeding element,	0.5×3.5	20.8	LTE 42/43	20 dB	70 %	< 0.0125	150×75	-

Reference	No. of Elements	Antenna Type	Element Size (mm)	Element separation	Bandwidth (GHz)	Isolation (dB)	Element Efficiency	ECC at resonance	Ground Size (mm ²)	Method Of ECC Calculation
		an inverted U-shaped	17.4 × 6							
[5]	4	self-decoupled antenna	20 × 6	73	LTE 42/43	17 dB	43 %	< 0.1	150 × 73	-
[10]	8	L-shaped slot antenna	9 × 7	19	NR Bands n77/n78/n79	12 dB	76 %	< 0.11	150 × 75	Measured Three-Dimensional Complex E-Field Patterns
[7]	8	inverted-F antenna with shorting branches and parasitic elements	13.9 × 7	16.6	n77/n78 (3.3–4.2 GHz), n79(4.4–4.9 GHz) LTE Band 46	10 dB	70 % 56 % 68 %	< 0.1	136 × 68	Measured 3D Complex E-Field Patterns
[11]	8	T-shaped and C-shaped slots	17 × 5.7	19	3.3 – 6	18 dB	-	< 0.05	150 × 75	Farfield Radiation Patterns
[12]	10	hybrid loop antenna	17.2 × 3.8	12	3.2–6.1	18 dB	78.4%	0.21	120 × 70	Farfield Radiation Patterns
[13]	8	open-slot antennas	28×7×1.8 (Ant. Pair)	32	3.3–5	10.8 dB	62 - 81%	< 0.15	145 × 75	simulated radiated far field
[14]	10	Loop antenna	6.5 × 6	25	3.4 – 3.6	10 dB	65%	< 0.055	150 × 77	3D electric field patterns
[15]	6	Ring loop antenna	13 × 28	19	2.3 – 6.5	20 dB	70%	< 0.01	150 × 75	S - Parameter
[16]	8	inverted L-shaped monopole	4.6 × 5.6	31	3.3 – 3.7	15 dB	50 – 75%	< 0.1	136 × 68	Farfield Radiation Patterns

II. PROPOSED MIMO ARRAY DESIGN

A. Antenna Element

Figure 1 depicts the geometry of the proposed antenna, while Table 2 lists the antenna's dimensions. The proposed antenna element is a ring loop antenna, where the Space-filling curve of order 3 was used to design the loop (Hilbert curves) [17]. Hilbert curve is used to reduce the size of the antenna as well as to get multiple resonances to cover multiple bands: LTE band 42 (3.4 -3.6 GHz), LTE band 43 (3.6 -3.8 GHz), and LTE band 46 (5.15 -5.925 GHz). The total length of the Hilbert curve increases when increasing the iteration stage while keeping the overall space of the entire geometry fixed. So that we selected order 3 which enables us to design the antenna element with dimensions 17.4 × 12.8 mm with a width of 0.9 mm. The proposed loop antenna consists of a loop strip with a length of about 0.5 λ. The loop strip is meandered to save space and bent to generate four resonant modes, the 0.5λ, 1 λ, 1.5 λ modes,

and a higher mode 2λ mode. The proposed antenna is a dual-band antenna to cover the LTE bands 42/43 and LTE band 46 for the 5G cell phone applications.

The antenna element is constructed as a stacked antenna as shown in Figure 1 (a), where it consists of a lower printed loop antenna fabricated from copper material shown in Figure 2(b) and an upper loop antenna with dimensions shown in Figure 2(c), and between them, two layers of an FR4 dodecagon substrate, each of 1.5mm thickness, are inserted. Furthermore, as shown in Figure 1 (a), the dodecagon design was deliberately chosen since it has 12 sides, allowing the antenna to be rotated by 30 degrees.

TABLE 2: Dimensions of ring loop antenna

Item	Value	Item	Value
L	17.4 mm	W1	1.2 mm
W	12.8 mm	W2	4.8 mm
L1	4.6mm	W3	5.1 mm
L2	8.9mm	W4	6 mm
L3	3.1 mm	W5	0.9 mm
L4	4.3 mm	W6	2.6 mm

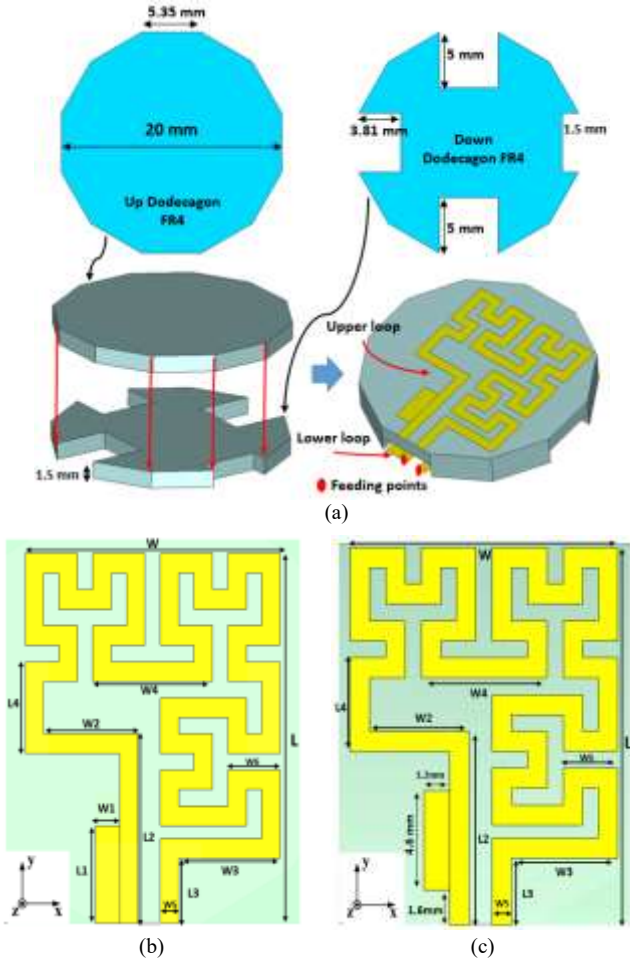


Fig. 1. The proposed antenna Geometry, (a) The stacked loop antenna with formed FR4 substrate, (b) Lower loop antenna, (c) Upper loop antenna

In addition, the down layer of dodecagon substrate is made by cutting some areas, with the impact of producing the substrate taken into consideration. The resonant frequency and bandwidth are shifted as the substrate is formed. Figure 2 shows the design steps of the main element where step1: the loop antenna is printed on the FR4 substrate with a thickness of 1.5 mm and ground plane. Step 2: Add a layer of dodecagon substrate with a thickness of 1.5 mm. step 3: etching some parts from the dodecagon substrate for SMA terminals and for enhancement of the S-parameter. Step 4 add another layer of dodecagon FR4 substrate that justified the position of the resonance frequencies. Step 5 printing another loop antenna on the upper dodecagon FR4 substrate that enhanced the matching of the antenna through the desired bands.

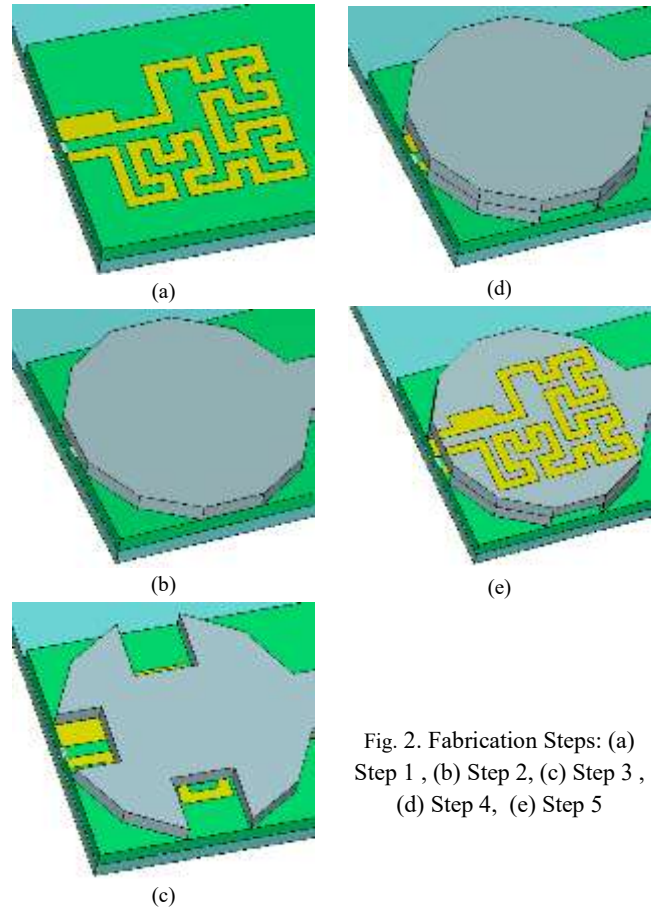


Fig. 2. Fabrication Steps: (a) Step 1 , (b) Step 2, (c) Step 3 , (d) Step 4, (e) Step 5

Figure 3 shows the S-Parameter (S_{11}) for the main antenna element for each design step shown in figure 2.

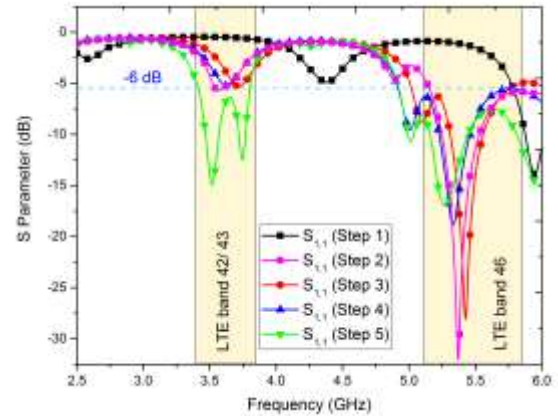


Fig. 3. S-Parameters of the main antenna element according to figure 2

The surface current density distributions of the proposed antenna are shown in Figures 4 (a) and (b) at resonance frequencies of 3.6 GHz and 5.5 GHz, respectively.

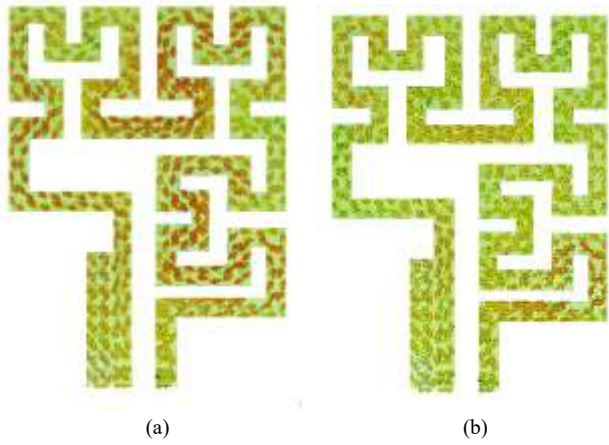


Fig. 4. Surface current density distributions of the antenna at (a) 3.6 GHz, and (b) 5.5 GHz.

Table 3 shows a parametric study on two elements array (Ant 1 and Ant 2) with different orientation angles, where Ant 1 is fixed orientation and Ant 2 is rotated by angle 30° . To show the effect of the orientation angle on the isolation (S_{21}) and ECC values calculated from both the S parameter and Far field Radiation Patterns. From this figure, it is concluded that the orientation angles 120° and 330° are the optimum angles. Table 4 shows the spacing effect between two elements array on coupling. From this table, it can be concluded that when the distance between the two adjacent elements is reduced the isolation is reduced and the ECC value is increased. Also, when the distance between the two-dodecagon substrate reduced to reach zero, the isolation reached 18 dB and 23 dB in the LTE band 42/43 and LTE band 46 respectively. It is a very good isolation value, but for the proposed array, there is a distance between the adjacent elements that can connect the SMA connector for measuring purposes. Figure 5 shows the directivity and efficiency of the main element. The proposed antenna element covers

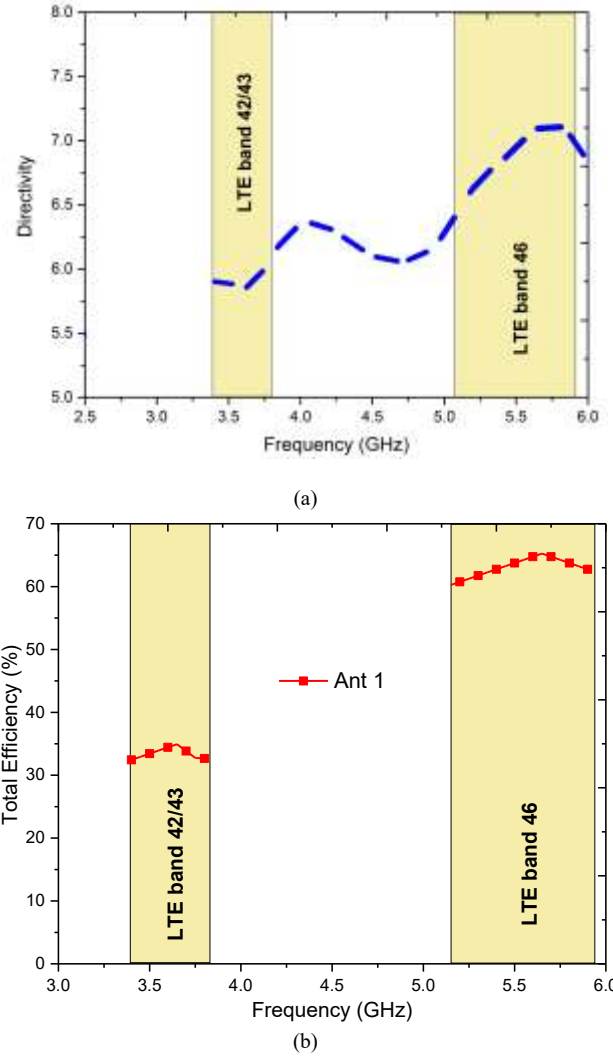
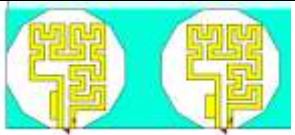

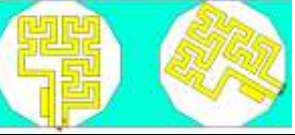
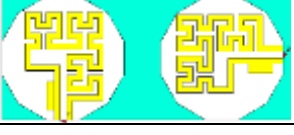


Fig. 5. Main antenna element (a) Directivity (b) Total efficiency

TABLE 3 A parametric study on two elements array with different orientation angles

Angle	Isolation (S_{21}) dB		ECC from the S parameter		ECC from Far field Radiation Patterns	
	LTE 42/43	LTE 46	LTE 42/43	LTE 46	LTE 42/43	LTE 46
 0°	22.9	26.8	0.0011	0.0015	0.19	0.025
 30°	27	26.1	0.0016	0.0015	0.09	0.03
 60°	25.8	24.76	0.00198	0.00263	0.1	0.016
 90°	29.04	27.17	0.00054	0.0016	0.19	0

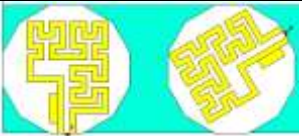
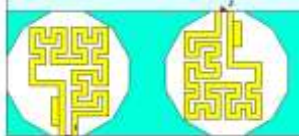
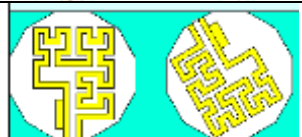



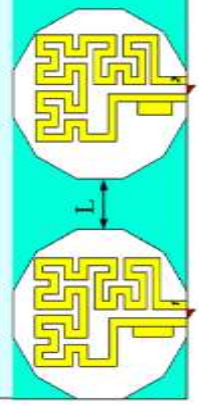
Angle		Isolation (S_{21}) dB		ECC from the S parameter		ECC from Far field Radiation Patterns	
		LTE 42/43	LTE 46	LTE 42/43	LTE 46	LTE 42/43	LTE 46
	120°	37.7	27.4	0	0.0009	0.28	0
	150°	33.3	24.4	0	0.00087	0.33	0.03
	180°	25.3	22.62	0.0023	0.0047	0.41	0.026
	210°	25	18.48	0.0036	0.0078	0.22	0.024
	240°	25.6	17.1	0.004	0.01	0.2	0.037
	270°	26.5	17.6	0.003	0.008	0.3	0.027
	300°	26.3	19	0.0038	0.0033	0.32	0.01
	330°	30.4	21.7	0.001	0.0014	0.14	0.019

TABLE 4 the spacing effect between two elements array on coupling

Distance (L) in (mm)		Isolation (S_{21}) dB		ECC from Far field Radiation Patterns	
		LTE 42/43	LTE 46	LTE 42/43	LTE 46
	5	28	24	0.095	0.06
	4	27	25	0.11	0.061
	3	25.6	25.9	0.14	0.061
	2	23.6	26	0.18	0.061
	1	21.4	25	0.21	0.06
	0	18	23	0.28	0.06

B. Ten Port MIMO Array Structure

Figure 6 illustrates the architecture and dimensions of the proposed 10 port array. The proposed design architecture includes dimensions of 150 mm × 80 mm × 8 mm. The mobile phone battery and the LCD screen are both made of metal. The battery is designed to be in the lower-left corner of the mobile phone, with dimensions of 50 × 70 × 6 mm³. The battery block is specified as copper in the simulation. The two hatched blocks in Figure 6 (a), each has dimensions of 7 mm × 35 mm, are designated for housing 3G/4G antennas, it will be copper areas.

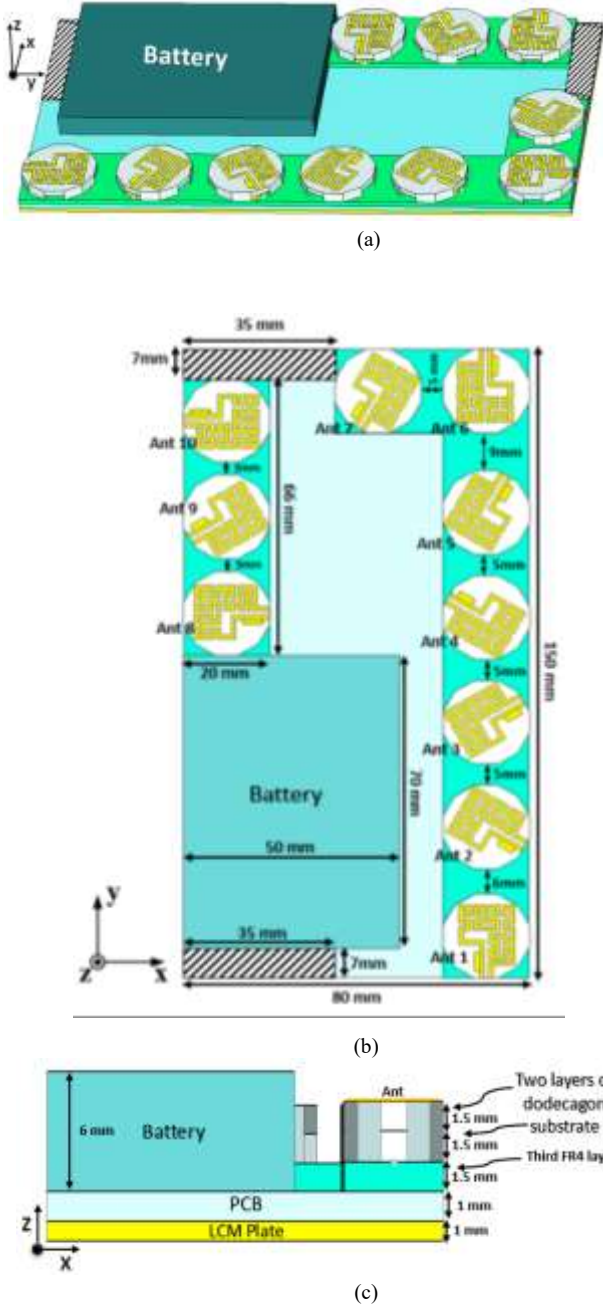


Fig. 6. Architecture and detailed dimensions of the proposed array (a) Phone geometry, (b) top view, and (c). Side view

The simulated S-parameter of the proposed array was calculated using the full-wave Computer Simulation Technology (CST) microwave studio version 2021. Figure 7 investigates the simulated S-parameter, where the reflection coefficients of the 10 antenna elements are shown.

The proposed antennas cover both the LTE band 42/43 and band 46 below -6 dB bandwidth. Also, the isolation between every two adjacent antennas is investigated in Figure 7 (b), and very good isolations are achieved. For LTE band 42/43, the isolation values ranged from -22 dB to -43 dB, whereas for LTE band 46, the values ranged from -22 dB to -50 dB, achieving good spatial diversity.

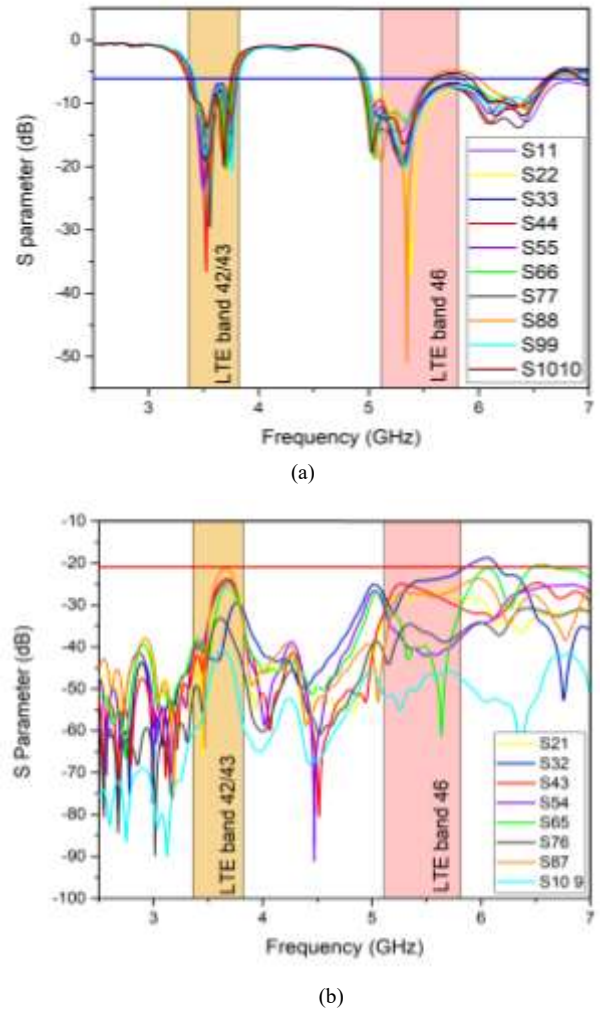
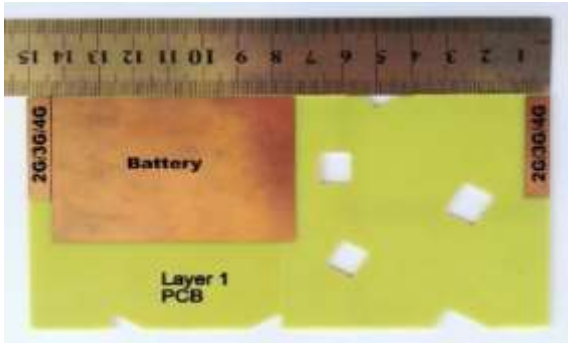
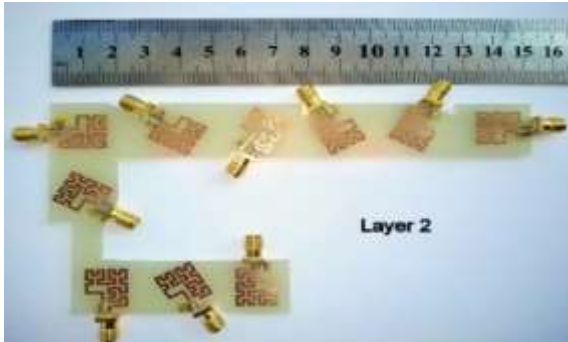


Fig. 7. The Simulated S-Parameter of the proposed array, (a) Reflection coefficient, and (b) Isolation between the adjacent ports.

Figure 8 shows the manufactured 10 port MIMO array, which is made up of four layers. The PCB layer is the first layer, which is made of FR4 material (loss tangent 0.02 and relative permittivity 4.4). From the bottom, a layer of copper covers it, while the copper just covers the battery and 3G/4G areas from the top. The second layer is a substrate layer made of FR4 material, printed on its top ten copper antennas, with ten SMA connectors for testing. The third layer is made up of 10 interconnected formed dodecagons. Ten loop antennas are printed on a ten dodecagon FR4 substrate as the fourth layer.



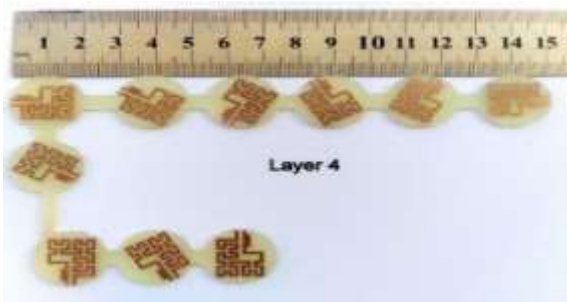
(a)



(b)



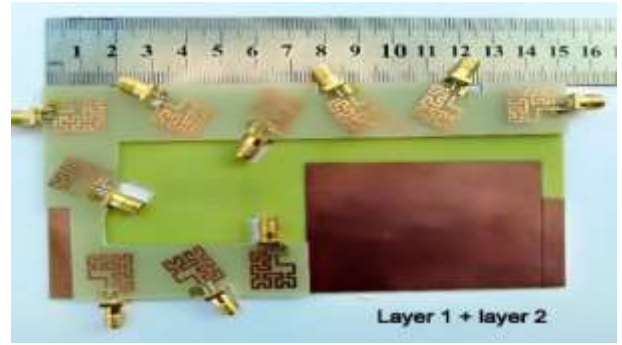
(c)



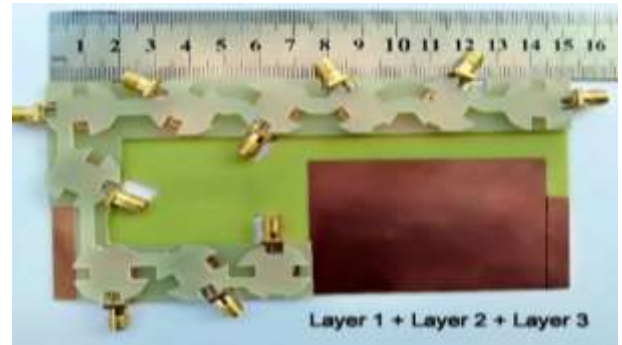
(d)

Fig. 8. The fabricated layers, (a) layer1, (b) layer 2, (c) layer 3, (d) layer4.

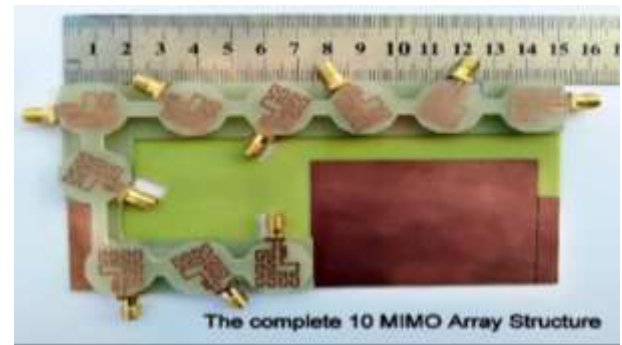
The proposed MIMO array design's integration steps are shown in figure 9. Figure 9 (a) investigates the first step, in which the second layer is placed on the PCB layer, Figure 9 (b) depicts the instruction of the third layer over the second and first layers, and Figure 9 (c) depicts the complete structure of the 10 MIMO antenna array. The 10 antenna components are glued together and printed on the same substrate layer's identical surface. It's worth noting that the phone's LCM plate is considered by the ground plane.



(a)



(b)



(c)

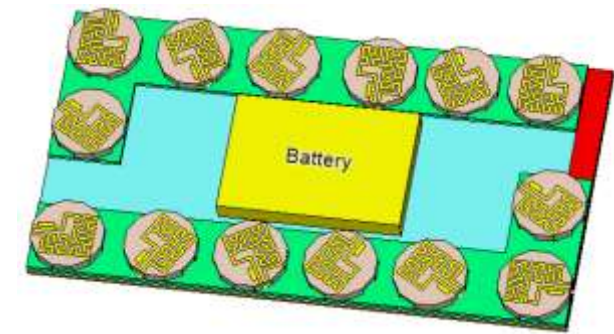
Fig. 9. Integration Steps, (a) The second layer on the PCB layer, (b) The third layer over the second and first layers, and (c) the complete structure of the 10 MIMO array.

C. 14 Port MIMO Array Structure

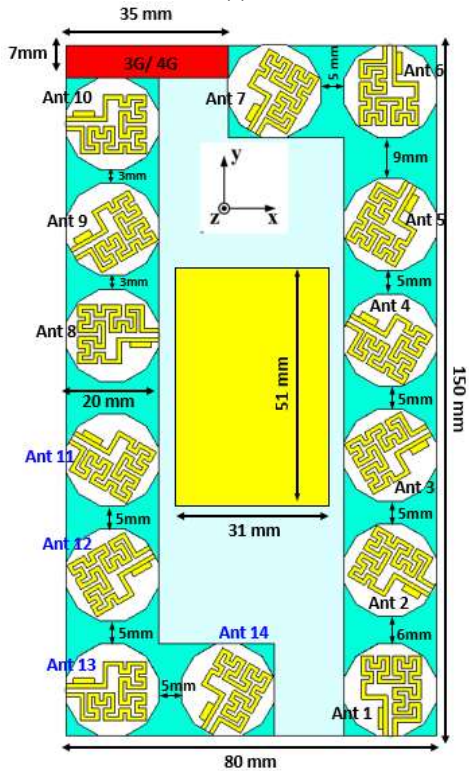
In this section, we modified the 10-port array to be 14 port array of the same size as the phone. Achieving good ECC values and isolation. The architecture and dimensions of the suggested 14 antenna array are shown in Figure 10. Where the architecture and dimensions of the proposed mobile phone are the same as mentioned in section 2.2. It is used the same type of antenna element (ring loop antenna) with the same dimensions. But we removed the battery block from the lower-left corner to be in the center for exploiting this area by adding four antenna elements (Ant 11 - Ant 14) with a spacing of 5 mm between them to keep the isolation.

The dimensions of the battery used in the fourteen-port array will be different from the battery used in the ten port array. The battery dimensions will be $31 \times 51 \times 6$ mm [18]. Besides that, those antennas were added at certain angles to reduce the mutual coupling between them. Where Ant 11 is rotated by angle -30° from the positive x-axis, Ant 12 is rotated by angle 210° from the positive x-axis, Ant 13 is

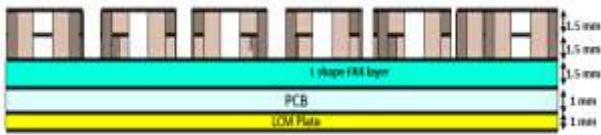
directed toward the positive x-axis, and Ant 14 is rotated by angle 60° from the positive x-axis.



(a)



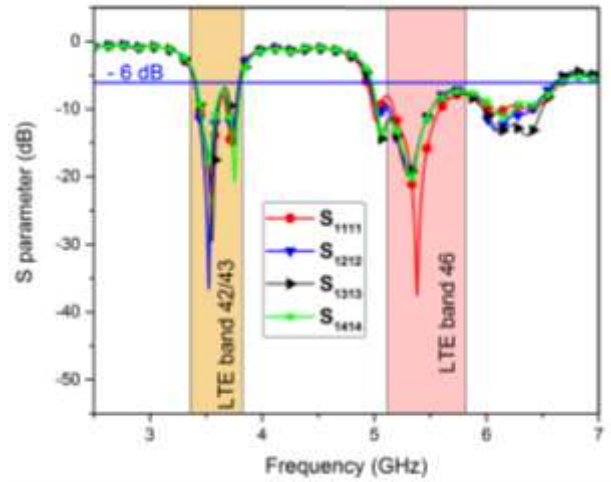
(b)



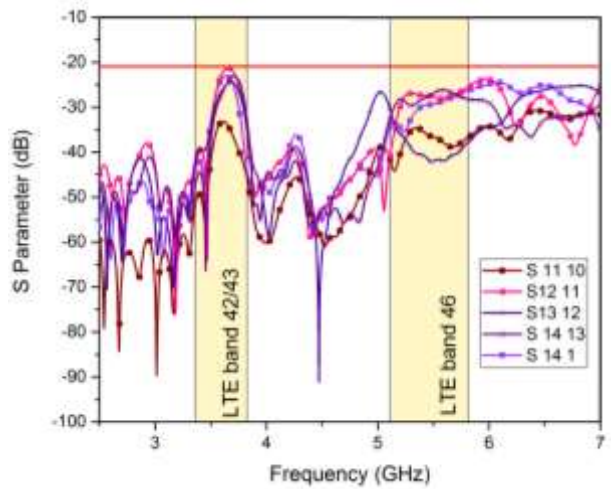
(c)

Fig. 10. Architecture of the proposed 14-port array (a) Geometry of the mobile phone, (b) Top view, (c) Side view

Figure 11 investigates the simulated S parameter for only the added ports (Ant 11 – Ant 14), using the CST microwave studio version 2021. Furthermore, Figure 12 shows the surface current distribution for the 10 port MIMO array as in figure 12 (a), and 14 port array as in figure 12 (b), also the current distribution for the single element is shown in figure 12 (c).

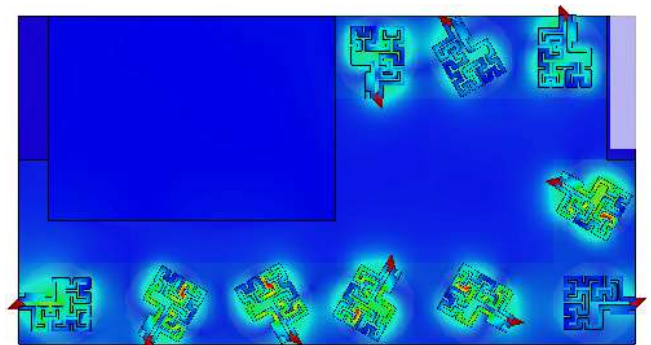


(a)

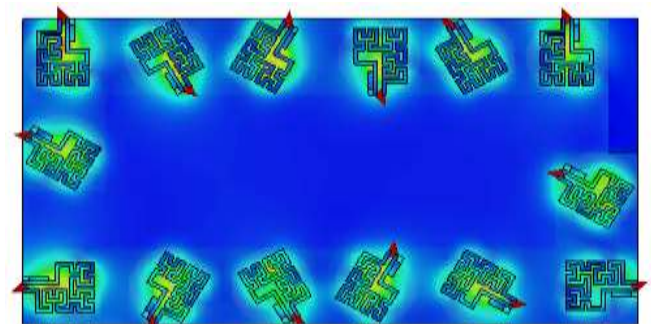


(b)

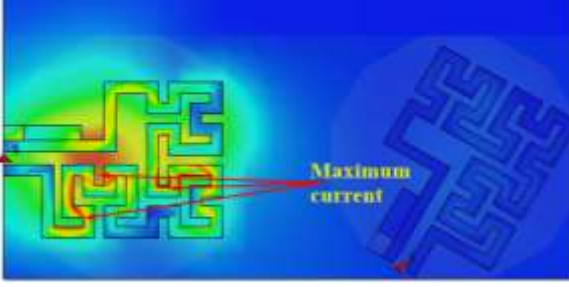
Fig. 11. The Simulated S-Parameter, (a) reflection coefficient of Ant 11 – Ant 14, (b) Isolation between adjacent ports (Ant 11 – Ant 14)



(a)



(b)



(c)

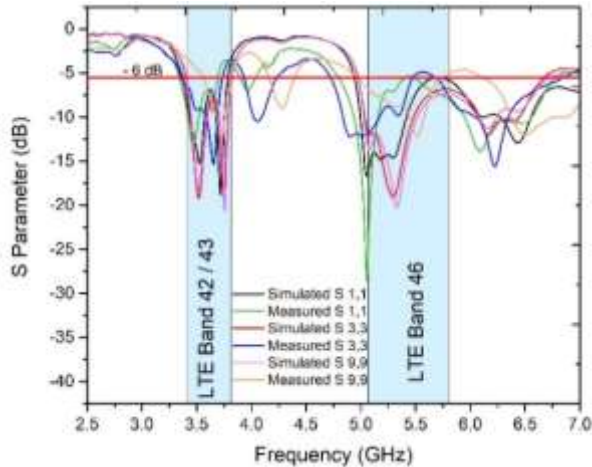
Fig. 12. Surface current distribution at 3.5 GHz (a) 10 port MIMO array (b) 14 port MIMO array, (c) single element

III. RESULTS AND DISCUSSION

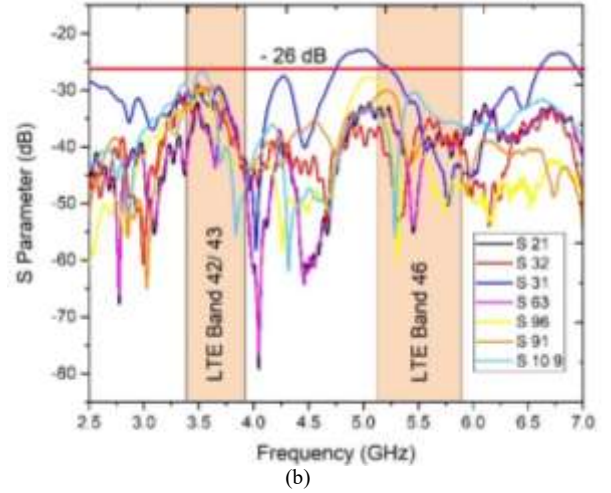
The proposed 10 port MIMO array was built and tested as illustrated in Fig. 9. For briefly, only six antennas were used in the tests, Ants 1, 2, 3, 6, 9, and 10. By comparing computed and measured data, the performance of the suggested dual-band MIMO array will be described in this part. On the other hand, only the simulated results for the 14 port array are considered. The observed S-parameters (isolation and reflection coefficients), the ECC parameter, and Ergodic Channel Capacities will be reviewed. Also, the features of radiation patterns and SAR values are studied.

A. S Parameters

Figure 13 illustrates the proposed prototype's measured S-parameters. As observed, the measured S-parameters correspond well with the simulated equivalent. Even so, there are some minor variations between the simulated and measured results. This might be related to minor fabrication tolerances or inaccuracies, as well as the SMA connector's insertion. Fig. 13 (a) depicts the proposed dual-band MIMO array's measured and computed reflection coefficients.



(a)



(b)

Fig.13. Measured S parameters, (a) Reflection coefficients & simulated results (b) Isolation.

The lower band's fraction bandwidths ranged from (8.5 - 14 %), while the upper band's fraction bandwidths ranged from (10 to 47.61 %), covering both LTE bands 42/43 and 46. Fig. 13 (b) depicts the equivalent isolations between the neighboring antennas of the dual-band antenna components. The isolation was below - 26 dB, as indicated in this figure. The measurement results reveal that the suggested MIMO architecture has good isolation and reflection coefficients, allowing it to completely cover LTE bands 42/43 and 46.

B. MIMO Performances

• Total Efficiency

The simulated overall efficiencies for the 14 antennas are shown in Figure 14. The acquired results were achieved when only one antenna element was excited and the remaining thirteen antennas were all matched. Efficiencies for the lower band (LTE bands 42/43), as indicated in this graph, were about 40 %. Furthermore, overall efficiencies for the higher band (LTE Band 46) are about 65 %. The total efficiency evaluation has been influenced by mutual coupling losses, mismatching, and radiation.

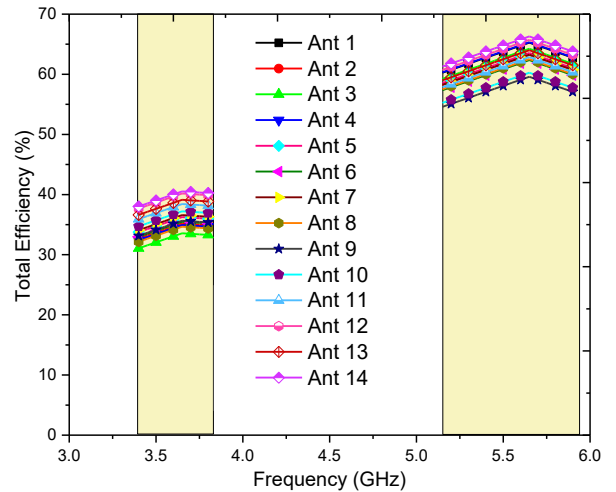


Fig. 14. Total efficiencies for the proposed dual-band 14 port MIMO array

• Envelope Correlation Coefficient (ECC)

The ECC coefficient is calculated from the S parameter based on formula (1) [19]. For the two LTE bands (LTE band 42/43 and LTE band 46), Fig. 15 shows the ECC

values for nearby antenna pairs. In this figure, the ECC values calculated from the S parameter are less than 0.005 in LTE band 42/43 and less than 0.006 in LTE band 46, and then calculated from three-dimensional far-field radiation patterns are < 0.2 in LTE band 42/43 and < 0.12 in LTE band 46, which meets the acceptable ECC criteria of less than 0.5. Due to the asymmetry of the main element rotating the antenna elements reduces the coupling between the adjacent antennas. As a result, we get a small ECC value. So that, the suggested 14 x 14 array can attain an appropriate variety of features based on these results.

$$\rho_{ab} = \frac{|s_{aa}^* s_{ab} + s_{ab}^* s_{bb}|^2}{(1 - |s_{aa}|^2 + |s_{ba}|^2)(1 - |s_{bb}|^2 + |s_{ab}|^2)} \eta_a \eta_b \quad (1)$$

For a more accurate calculation of ECC. It can be calculated from three-dimensional far-field radiation patterns [20] as:

$$\rho_{e,ij} = \left| \frac{\int_0^{2\pi} \int_0^\pi (\text{XPR} \cdot E_{\theta i} \cdot E_{\theta j}^* \cdot P_\theta + \text{XPR} \cdot E_{\phi i} \cdot E_{\phi j}^* \cdot P_\phi) \sin(\theta) d\theta d\phi}{\sqrt{\prod_{k=i,j} \int_0^{2\pi} \int_0^\pi (\text{XPR} \cdot E_{\theta k} \cdot E_{\theta k}^* \cdot P_\theta + \text{XPR} \cdot E_{\phi k} \cdot E_{\phi k}^* \cdot P_\phi) \sin(\theta) d\theta d\phi}} \right|^2 \quad (2)$$

where $\text{XPR} = P_V/P_H$ is the cross discrimination ratio between vertical and horizontal polarized power components, and $E_{\theta i}$, $E_{\theta j}$, $E_{\phi i}$, $E_{\phi j}$ are the field components of i and j ports in elevation and azimuth directions, respectively. P_θ and P_ϕ are the elevational and azimuthal angular power spectrum (APS) distribution.

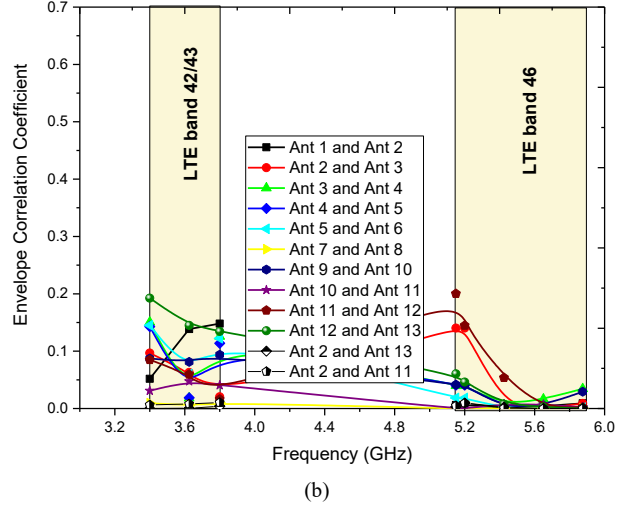
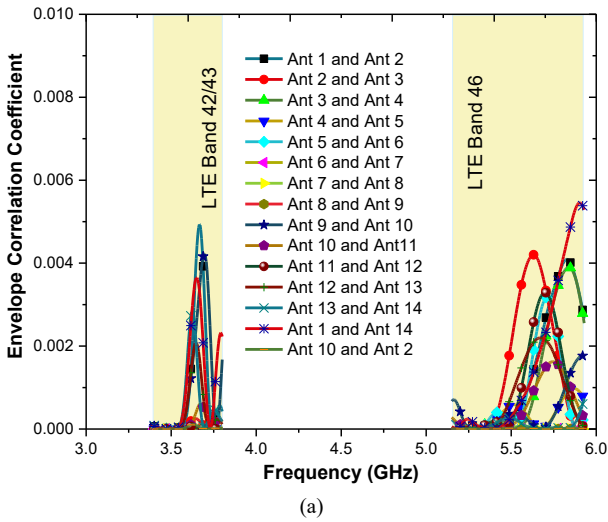


Fig. 15. ECC parameter for the proposed dual-band 14 port MIMO Array (a) from S parameter (b) Farfield Radiation Patterns

- Channel Capacity

Typically, the Shannon formula (3) is used to calculate the ergodic channel capacity of a MIMO system. When estimating the MIMO array's channel capacity, the MIMO system's channel model should be chosen first, with the ray-tracing model or a comparable statistical model being utilized in most cases. As a result, the correlation matrix approach is used to compute the channel capacity of the proposed 10×10 and 14×14 MIMO arrays [9].

$$C = \log_2 \det \left(\mathbf{I} + \eta \frac{\text{SNR}}{K} \mathbf{H} \mathbf{H}^H \right) \quad (3)$$

where \mathbf{I} is the identity matrix, SNR is the mean SNR. \mathbf{H} is the channel matrix, and $\mathbf{H} \mathbf{H}^H$ is the Hermitian transpose of the matrix. The matrix $\mathbf{H} \mathbf{H}^H$ has a rank of K . The key to estimating the channel capacity using the correlation matrix approach is to find out the channel matrix $[\mathbf{H}]$ using the statistical method. The antennas on the transmitter and receiver sides of the proposed MIMO array are distanced by a quarter wavelength under non-line of sight conditions. Figure 16 shows the calculated capacity for the proposed 10×10 and 14×14 MIMO arrays. Considering simulated efficiencies and averaging 1000000 Rayleigh fading realizations with SNR equal 20 dB in the identically and independently dispersed propagation condition. For the lower band (LTE 42/43), the computed channel capacities of 10×10 and 14×14 arrays are roughly 27.1 bps/Hz and 40 bps/Hz respectively. But, for the higher band (LTE 46), the computed capacities of 10×10 and 14×14 arrays are roughly 57.6 bps/Hz and 72 bps/Hz respectively. When the number of antenna elements is increased from 10 to 14, the channel capacity is increased by around 20%.

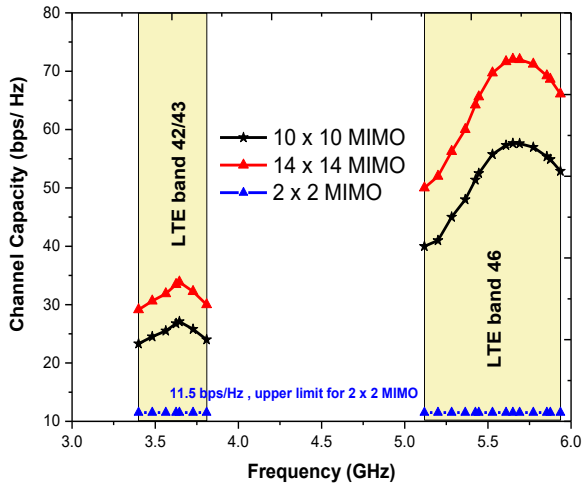


Fig. 16: Channel capacity of the proposed 10×10 and 14×14 MIMO arrays

- Diversity Gain (DG)

The following formula is used to compute the DG values (dB) [21].

$$DG = 10\sqrt{1 - |ECC|^2} \quad (4)$$

Figure 17 illustrates the proposed 14×14 MIMO array's DG values. In the LTE bands 42/43 and 46, due to the lower ECC values, the DG values are around 10 dB. Industry guidelines mandate that DG values be about 10dB to function better in real-world situations and provide better service. As shown in Figure 16, the proposed MIMO array is ideally suited to fulfill the need of industry standards.

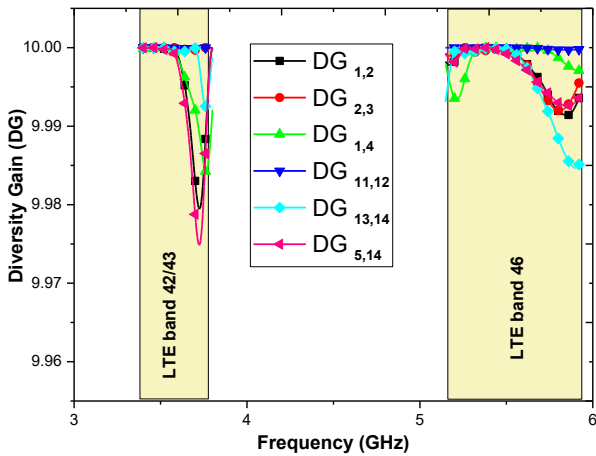


Fig. 17. Diversity Gain values for the Proposed 14×14 MIMO array

- Specific Absorption Rate (SAR)

The effect of the human body on the proposed array is also taken into account. In CST MWS, the built-in voxel model is used to simulate human tissues. The Gustav voxel model was used to explore the influence of human proximity on array performance.

Figure 18 investigates the simulated SAR values for the head phantom with the antenna array closer to the human head. The simulation is run with the human hand present, averaged over the volume of 10 g of tissue, according to the IEC/IEEE 62704-1 averaging method [22]. Fig. 18

demonstrates that the SAR values for ant 1, ant 3, ant 5, and 7 are 0.0097 - 0.0333 W/kg, which are lower than the maximum standard values. Where the maximum allowable level is 1.6 W/Kg averaged over 1 g of tissue and 2.0 W/Kg averaged over 10 g of tissue.

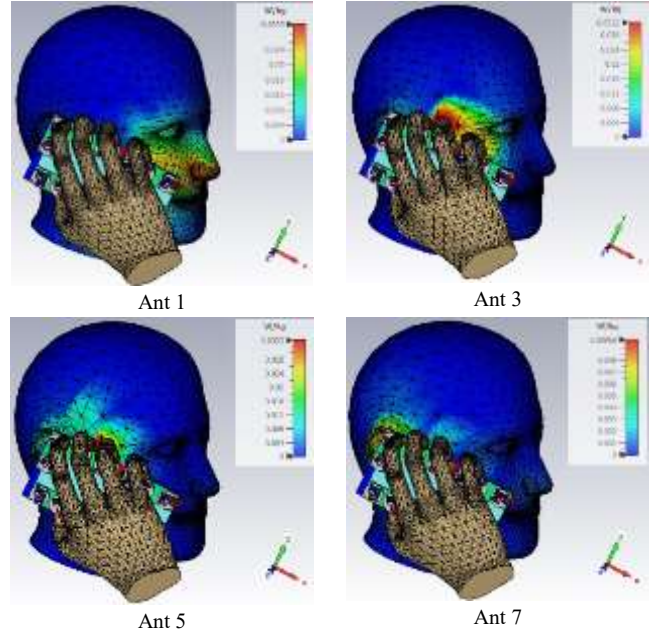
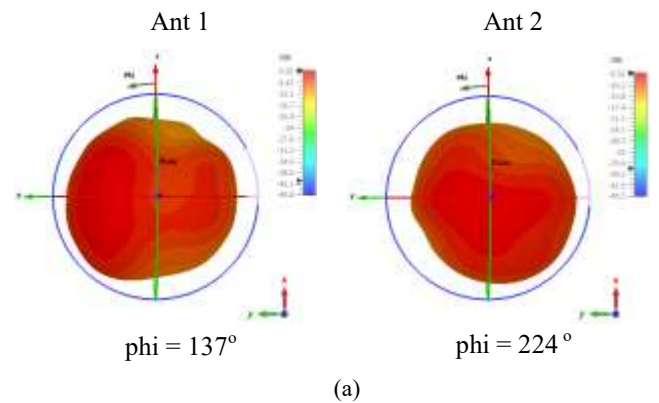


Fig. 18. Simulated SAR values at 3.5 GHz for ant1, ant 3, ant 5, and ant7

- Radiation pattern

Figure 19 investigates the 3D radiation patterns of the proposed antennas. For briefly, the radiation patterns of the Ant 1 and Ant 2 are presented at resonance frequencies 3.5GHz and 5.3GHz. As shown in Fig. 15 (a) and (b), The radiation patterns of the antennas are directed in different Phi angles and this is due to the different orientation angles of the antennas. Thereby demonstrating pattern diversity feature.



Ant 1

Ant 2

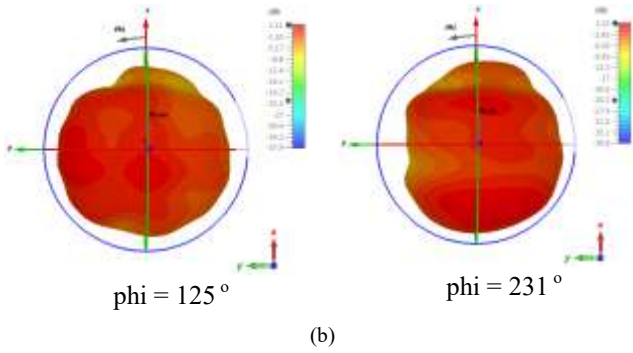


Fig. 19. Simulated 3D radiation patterns, (a) at 3.5 GHz, (b) at 5.3 GHz

- Effect of mobile frame

In this section, the effect of two types of mobile frames (plastic frame and metal ring frame) are investigated. Figure 19 shows the simulated design for the proposed 14×14 MIMO array with a plastic frame as in figure 20 (a) and a metal frame as in figure 20 (b).

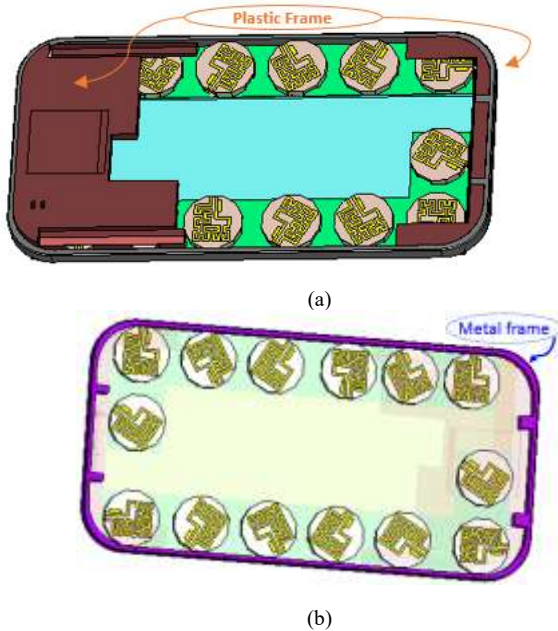
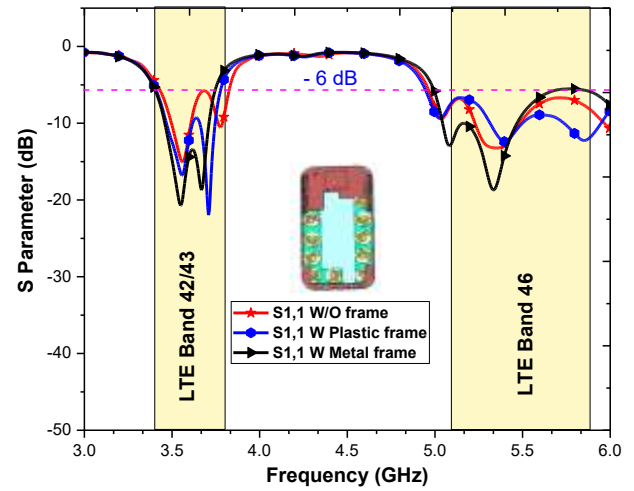
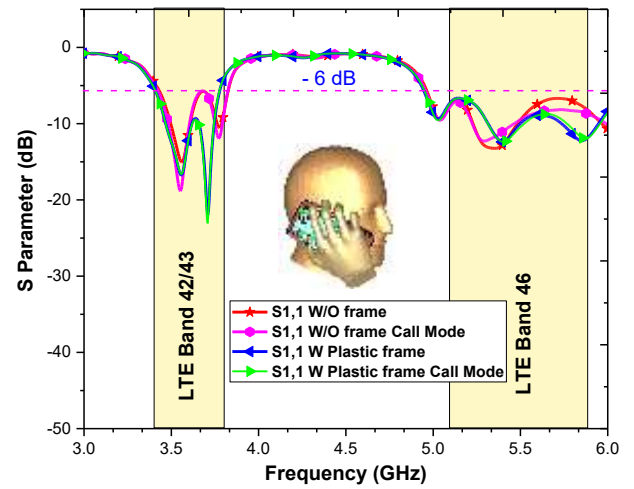


Fig. 20. Proposed 14×14 MIMO array with mobile Frame, (a) Plastic frame, (b) Metal Frame.

Figure 21 shows the effect of the frame insertion on the reflection coefficient of ant 1. From fig. 21 (a), it is observed that the plastic frame enhances the performance of ant 1 more than in the case without a frame. It fully covers both LTE band 42/43 and LTE band 46. But in the case of a metal frame, the reflection coefficient of ant 1 is affected by the metal. The bandwidth is reduced and did not cover the entire required bands. Besides that, fig. 21 (b) shows the effect of head phantom (call mode) on the reflection coefficient of ant 1 in the case of the mobile plastic frame and without a frame. It can be seen that in the case of without frame, the performance of Antenna 1 was slightly affected by the presence of the head phantom, especially in the higher band. But, in the case of a plastic frame, the reflection coefficient of ant 1 remained stable as it is with the present head phantom.



(a)



(b)

Fig. 21. Effect of frame insertion on the reflection coefficient of ant 1 (a) Absence of a head phantom, (b) In case of a head phantom

Figure 22 shows the effect of the plastic and metal frame on the antenna efficiency. For briefly, only antennas 1, 2, and 3 have been shown. From this figure, in the case of using the plastic frame, the efficiency of the antennas changed by a very small value. But in the case of using the metal frame, it is noted that the efficiency of the antennas was affected. From figure 22, the efficiency of ant1 equals 61.78 % without a frame and reached 63.26 % with a plastic frame and reduced to 59.5 % with metal frame. Also the efficiency of ant 2 in case of no frame is equal 65.9 % and in case of plastic frame is 65.9 % with no change, but in case of metal frame, the efficiency reduced to 51.3 %.

Furthermore, figure 23 shows the ECC values for three adjacent antennas 1,2, and 3 under the effect of frame insertion, whereas table 5 shows the ECC values between ant 1&2 and ant 2&3 in three cases.

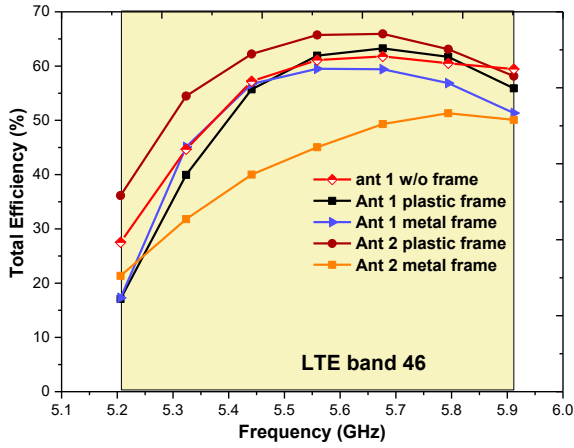
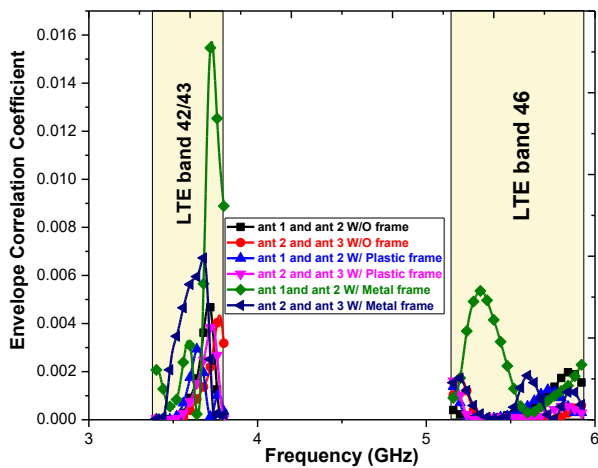


Fig. 22. Total Efficiency for the proposed array under frame effect

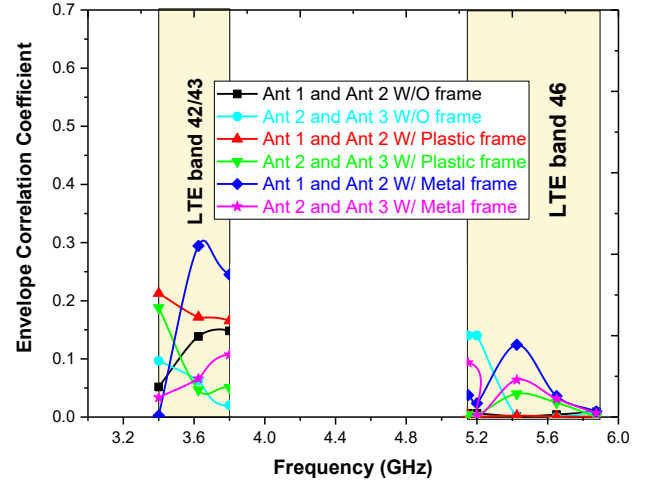
TABLE 5: The ECC values under the effect of frame insertion

Case / ECC from S-Parameter	ECC between ant 1 and ant 2	ECC between ant 2 and ant 3
Without frame	0.005	0.0043
With plastic frame	0.0029	0.0039
With metal frame	0.0154	0.0067
Case / ECC from Farfield Radiation Patterns	ECC between ant 1 and ant 2	ECC between ant 2 and ant 3
Without frame	0.15	0.14
With plastic frame	0.18	0.09
With metal frame	0.29	0.1

From table 5, it is indicated that the frame insertion also affected the ECC values, where in the case of the plastic frame, the ECC values are reduced than in the case of no frame, but in the case of the metal frame, the ECC values are increased than the other cases. As a result, the plastic frame improves the performance of the system, unlike the metal frame, which affects it.



(a)



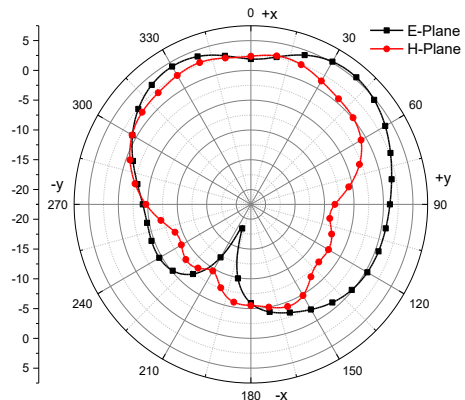
(b)

Fig. 23. ECC values for the proposed array under frame (a) ECC from S-Parameter (b) ECC from Farfield Radiation Patterns

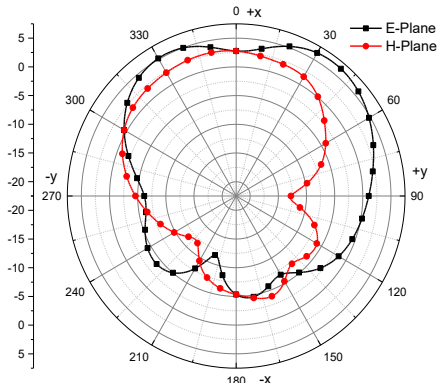
Figure 24 presents the effect of the frame insertion on the radiation pattern for the proposed array at 3.5 GHz. For briefly, only the 2D radiation pattern of ant 1 is presented. From this figure, it can be indicated that the radiation patterns of the proposed array are affected by the metal frame more than the plastic frame. Table 6 states the direction of the main lobe for ants 1-3. In the case of the plastic frame, it can observe that the direction of the main lobe of ant 1 and ant 3 are not affected, but ant 2 changed by a small difference angle of 7° . On the other hand, in the case of the metal frame, ant1 is slightly affected, but ants 2, and 3 are highly affected compared to those without a frame case. Where. The main lobe of ant 2 and ant 3 have different angles 52° and 52° respectively.

TABLE 6: Main lobe direction of ants 1-3 under frame insertion

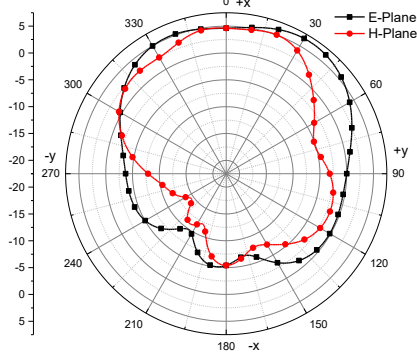
Case	Main lobe direction		
	ant 1	ant 2	ant 3
Without frame	Phi = 37°	Phi = 17°	Phi = 347°
Plastic frame	Phi = 37°	Phi = 24°	Phi = 346°
Metal frame	Phi = 32°	Phi = 325°	Phi = 29°



(a)



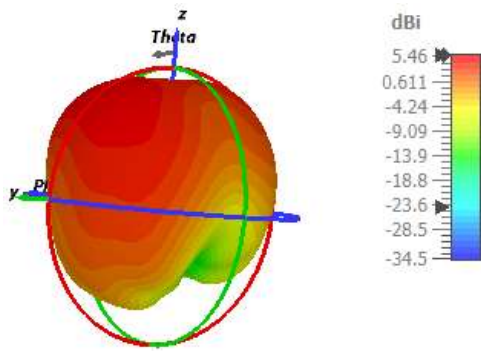
(b)



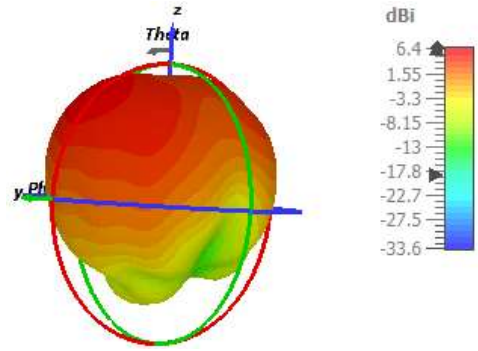
(c)

Fig. 24. 2D radiation pattern at 3.5 GHz for ant1 ant3 under frame effect: (a) Ant 1 w/o frame, (b) Ant 1 with plastic frame, (c) Ant 1 with metal frame

Figure 25 investigates the 3D radiation pattern for ant 1 at 3.5 GHz under the effect of frame insertion. Figure 25 (a) shows the case without a frame, where the radiation pattern of ant 1 has large back radiation. On the other hand, fig. 25 (b) shows the plastic frame case, the radiation pattern of ant 1 becomes more directive with lower back radiations. From all the previous results, the plastic frame is the preferred in smartphone designs



(a)



(b)

Fig. 25. 3D radiation pattern for ant 1 at 3.5 GHz (a) Without a frame, (b) With a plastic frame.

IV. PERFORMANCE COMPARISON

Table 7 shows a comparison between the proposed MIMO arrays and those previously reported for mobile handsets. From this Table, The proposed design can support dual-band massive MIMO covering LTE bands 42/43 band 46, while references [5], [8], and [9], do not cover LTE band 46. It has a large MIMO order of 14×14 , achieving a higher capacity of 72 bps/Hz through LTE band 46. It has exhibited the lowest isolation and ECC values in both LTE band 42/43 and LTE band 46 among all. This is a unique feature that all the references do not have.

V. CONCLUSIONS

In this paper, a dual-band ring loop antenna was proposed to cover the LTE bands 42/43 (3.4 – 3.8 GHz) and LTE band 46 (5.15 – 5.925 GHz). Two designs of ten port and fourteen port Massive Multi-Input Multi-Output (MIMO) arrays were proposed for 5G cellphone applications. The proposed arrays were designed with changing the battery position and exploiting the space to add more antennas. The proposed ten port array was manufactured and tested. The proposed designs achieved good isolation below -26 dB to -40 dB, ECC calculated by two methods from S parameter are less than 0.005 in LTE band 42/43 and less than 0.006 in LTE band 46, and then calculated from far-field radiation patterns are < 0.2 in LTE band 42/43 and < 0.12 in LTE band 46. . Also, the channel capacities were attained, the 10×10 MIMO achieved 57.6 bps/Hz, and the 14×14 MIMO achieved 72 bps/Hz. Furthermore, SAR, DG, and the effect of frame insertion on the proposed array were also discussed.

TABLE 7 A comparison of the proposed MIMO arrays with other References.

Ref.	Ground Size (mm ²)	-6 dB Bandwidth (GHz)		Total efficiency (%)		ECC		Capacity (bps/Hz) SNR=20dB		MIMO Order
				LTE 42/43	LTE 46	LTE 42/43	LTE 46	LTE 42/43	LTE 46	
[6]	150×80	LTE 42/43	LTE 46	41-82	47-79	< 0.15	< 0.1	37	29.5	8 × 8 (LB), 6 × 6 (HB)
[3]	150×75	LTE 42	LTE 46	50 -56	53 - 65	< 0.1	< 0.04	38.8	39.7	8 × 8
[9]	150×76.6	LTE 41/42 LTE 43	-	48 - 66, 44 - 59	-	< 0.2, < 0.05	-	38.3	-	8 × 8
[8]	150×75	LTE 42	-	60	-	< 0.0125	-	34	-	8 × 8
[5]	150×73	LTE 42	-	58	-	< 0.1	-	16–19	-	4 × 4
[23]	150×62.7	LTE 42/43	LTE 46	52.4-71.7	48.9-75.4	< 0.1	< 0.1	43.3	41.6	8 × 10
Proposed	150×80	LTE 42/43	LTE 46	40	65	< 0.005	< 0.006	27.1	57.6	10 × 10
						< 0.2	< 0.15	40	72	14 × 14

VI. REFERENCES

- [1] I. Al-Mejibli and S. Al-Majeed, "Challenges of using MIMO channel technology in 5G wireless communication systems," *2018 Majan Int. Conf.*, pp. 1–5, 2018, doi: 10.1109/mintc.2018.8472778.
- [2] W. Tang, S. Kang, J. Zhao, Y. Zhang, X. Zhang, and Z. Zhang, "Design of MIMO-PDMA in 5G mobile communication system," *IET Commun.*, vol. 14, no. 1, pp. 76–83, 2020, doi: 10.1049/iet-com.2018.5837.
- [3] H. Zou, Y. Li, C. Sim, and G. Yang, "Design of 8 × 8 dual-band MIMO antenna array for 5 G smartphone applications," *Int. J. RF Microw. Comput. Eng.*, vol. 58, no. 1, pp. 174–181, 2018, doi: 10.1002/mmce.21420.
- [4] L. Y. Rao and C. J. Tsai, "8-Loop Antenna Array in the 5 Inches Size Smartphone for 5G Communication the 3.4 GHz-3.6 GHz Band MIMO Operation," *Prog. Electromagn. Res. Symp.*, vol. 2018-Augus, pp. 1995–1999, 2018, doi: 10.23919/PIERS.2018.8598072.
- [5] Z. Ren, A. Zhao, and S. Wu, "MIMO Antenna With Compact Decoupled Antenna Pairs for 5G Mobile Terminals," *IEEE Antennas Wirel. Propag. Lett.*, vol. 18, no. 7, pp. 1367–1371, 2019, doi: 10.1109/LAWP.2019.2916738.
- [6] Y. Li, C. Y. D. Sim, Y. Luo, and G. Yang, "12-Port 5G Massive MIMO Antenna Array in Sub-6GHz Mobile Handset for LTE Bands 42/43/46 Applications," *IEEE Access*, vol. 6, no. c, pp. 344–354, 2017, doi: 10.1109/ACCESS.2017.2763161.
- [7] C. Y. D. Sim, H. Y. Liu, and C. J. Huang, "Wideband MIMO Antenna Array Design for Future Mobile Devices Operating in the 5G NR Frequency Bands n77/n78/n79 and LTE Band 46," *IEEE Antennas Wirel. Propag. Lett.*, vol. 19, no. 1, pp. 74–78, 2020, doi: 10.1109/LAWP.2019.2953334.
- [8] A. Zhao and Z. Ren, "Size Reduction of Self-Isolated MIMO Antenna System for 5G Mobile Phone Applications," *IEEE Antennas Wirel. Propag. Lett.*, vol. 18, no. 1, pp. 152–156, 2019, doi: 10.1109/LAWP.2018.2883428.
- [9] Y. Li, C. Y. D. Sim, Y. Luo, and G. Yang, "Metal-frame-integrated eight-element multiple-input multiple-output antenna array in the long term evolution bands 41/42/43 for fifth generation smartphones," *Int. J. RF Microw. Comput. Eng.*, vol. 29, no. 1, 2019, doi: 10.1002/mmce.21495.
- [10] H. D. Chen, Y. C. Tsai, C. Y. D. Sim, and C. Kuo, "Broadband Eight-Antenna Array Design for Sub-6 GHz 5G NR Bands Metal-Frame Smartphone Applications," *IEEE Antennas Wirel. Propag. Lett.*, vol. 19, no. 7, pp. 1078–1082, 2020, doi: 10.1109/LAWP.2020.2988898.
- [11] X. T. Yuan, W. He, K. D. Hong, C. Z. Han, Z. Chen, and T. Yuan, "Ultra-wideband MIMO antenna system with high element-isolation for 5G smartphone application," *IEEE Access*, vol. 8, pp. 56281–56289, 2020, doi: 10.1109/ACCESS.2020.2982036.
- [12] A. Singh and C. E. Saavedra, "Wide-bandwidth inverted-F stub fed hybrid loop antenna for 5G sub-6 GHz massive MIMO enabled handsets," *IET Microwaves, Antennas Propag.*, vol. 14, no. 7, pp. 677–683, 2020, doi: 10.1049/iet-map.2019.0980.
- [13] X. T. Yuan, Z. Chen, T. Gu, and T. Yuan, "A Wideband PIFA-Pair-Based MIMO Antenna for 5G Smartphones," *IEEE Antennas Wirel. Propag. Lett.*, vol. 20, no. 3, pp. 371–375, 2021, doi: 10.1109/LAWP.2021.3050337.
- [14] S. S. Aljaafreh *et al.*, "Ten Antenna Array Using a Small Footprint Capacitive-Coupled-Shorted Loop Antenna for 3.5 GHz 5G Smartphone Applications," *IEEE Access*, vol. 9, pp. 33796–33810, 2021, doi: 10.1109/ACCESS.2021.3061640.
- [15] J. Kulkarni, S. Dhabre, S. Kulkarni, C. Y. D. Sim, R. K. Gangwar, and K. Cengiz, "Six-Port Symmetrical CPW-Fed MIMO Antenna for Futuristic Smartphone Devices," *2021 6th Int. Conf. Conver. Technol. I2CT 2021*, pp. 1–5, 2021, doi: 10.1109/I2CT51068.2021.9418180.
- [16] M. Abdullah *et al.*, "Future Smartphone: MIMO Antenna System for 5G Mobile Terminals," *IEEE Access*, vol. 9, pp. 91593–91603, 2021, doi: 10.1109/ACCESS.2021.3091304.
- [17] J. Alber and R. Niedermeier, "On multidimensional curves with hilbert property," *Theory Comput. Syst.*, vol. 33, no. 4, pp. 295–312, 2000, doi: 10.1007/s002240010003.
- [18] A. Tatomirescu, E. Buskgaard, and G. F. Pedersen, "Reconfigurable Dual-Band Compact MIMO Antenna Destined For LTE," pp. 80–83, 2014.
- [19] G. Srinivas, D. Jabin, and A. K. Singh, "Multiband MIMO antenna with reduction in mutual coupling and ECC," *SCES 2014 Inspiring Eng. Syst. Glob. Sustain.*, pp. 1–5, 2014, doi: 10.1109/SCES.2014.6880064.
- [20] A. M. Elshirkasi, A. A. Al-Hadi, M. F. Mansor, R. Khan, and P. J. Soh, "Envelope correlation coefficient of a two-port mimo terminal antenna under uniform and gaussian angular power spectrum with user's hand effect," *Prog. Electromagn. Res. C*, vol. 92, no. January, pp. 123–136, 2019, doi: 10.2528/pierc19011006.
- [21] A. Kumar, S. K. Mahto, and R. Sinha, "Y-Shaped Antenna for 5G Enabled Gadgets and its MIMO for Smartphone Applications," *2020 URSI Reg. Conf. Radio Sci. URSI-RCRS 2020 - Proc.*, no. 1, pp. 12–14, 2020, doi: 10.23919/URSIRCRS49211.2020.9113521.
- [22] IEC/IEEE International Standard, *Determining the peak spatial-average specific absorption rate (SAR) in the human body from wireless communications devices, 30 MHz to 6 GHz - Part 1: General requirements for using the finite-difference time-domain (FDTD) method for SAR calculations.*, 2017.
- [23] Y. Li and G. Yang, "Dual-mode and triple-band 10-antenna handset array and its multiple-input multiple-output performance evaluation in 5G," *Int. J. RF Microw. Comput. Eng.*, vol. 29, no. 2, pp. 1–15, 2019, doi: 10.1002/mmce.21538.